nEXO Report
on
Muon Generation and Simulations

Regan Ross, Ubi Wichoski, Caio Licciardi

September 13, 2022

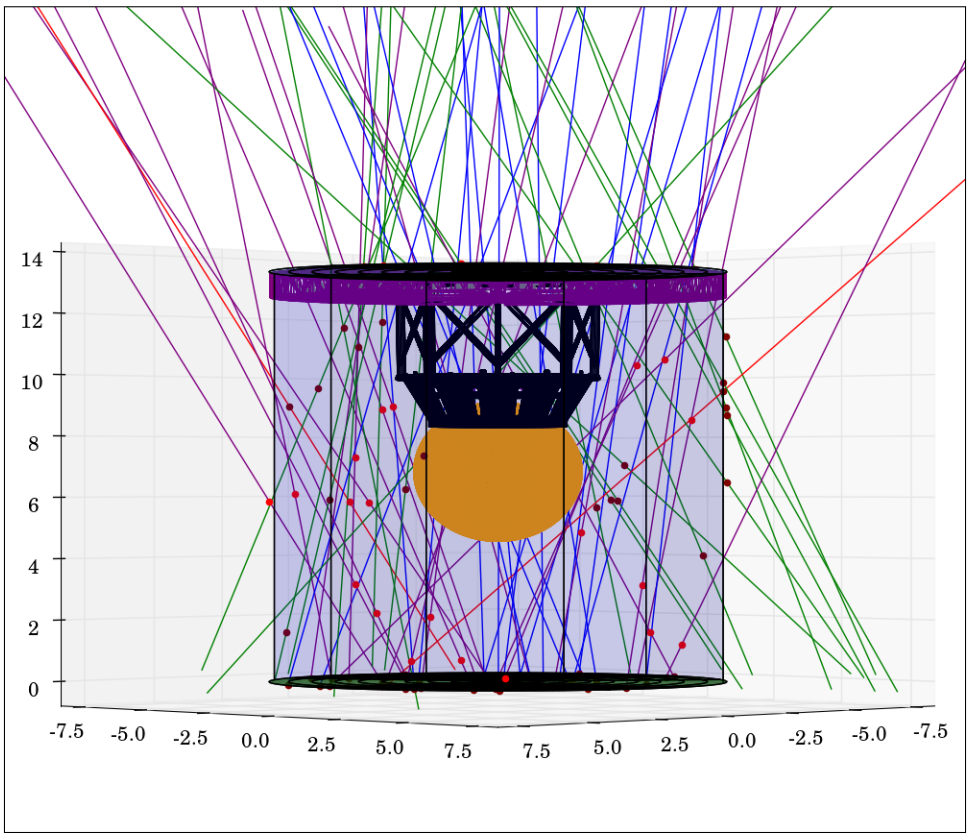

Abstract

nEXO is an experiment being designed to search for neutrino-less double beta decay ($0\nu\beta\beta$) in a 5000 kg liquid xenon time projection chamber (TPC) enriched to the isotope xenon-136. nEXO's $> 10^{28}$ year sensitivity reach to the $0\nu\beta\beta$ half-life requires extremely low backgrounds from external sources [1]. Backgrounds are dealt with in part by surrounding the TPC with an outer detector (OD) in the form of a cylindrical water tank. The OD serves both to passively shield from incident particles like gammas and neutrons and also to actively veto cosmogenic backgrounds by detecting the Cherenkov light of passing muons using photomultiplier tubes (PMTs). These muons undergo spallation processes on local nuclei sending neutrons into the TPC and activating the xenon.

In this paper, we discuss the simulation of incident cosmic muons in an underground setting. This work only reviews what is relevant to instantiating virtual beams of muons and their resultant Cherenkov light; other secondaries are beyond the scope of the work. However, this document is written so that the provided methods may be easily implemented in other work irrespective of the physics simulation tools deployed. Considerations of sampling uniformity and reasonable cutoffs are discussed along with analytical methods for determinining intersection points of muon tracks with various geometries. If properly implemented, one could deploy the methods elaborated herein to parametrize a muon beam for use in other simulation softwares, or to build a more customized Monte Carlo.

Acknowledgements

This work could not have been completed without the dedicated help of nEXO's Outer Detector collaboration. The code which resulted from these methods and ideas was refined through repeated trial and error—errors which, without the help of the collaboration, may have gone unnoticed. The authors are grateful for the help, feedback, and previous work provided by Soud Al Kharusi, Emma Klemets, Liam Retty, Remington Hill, Thomas Brunner, Erica Caden, Al Odian and others who provided judicious advice. Moreover, this work wouldn't have been possible without that which preceded it; all of the references within this text were useful in assembling these methods and data.

List of Figures

1 Rendering of nEXO's Outer Detector . . . 4
2 Atmospheric Muon Spectra; Energy vs. Zenith . . . 5
3 Mei & Hime's muon depth-intensity relation . . . 6
4 Cherenkov Spectrum for Through-Going Muons at SNOLAB . . . 8
5 Uniform vs. non-uniform radial distributions . . . 9
6 Maximum zenith angle criterion & simulation setup . . . 10
7 Muon Intersection Rate vs. Generation Disk Offset . . . 12
8 Through-going muon intensity from Mei & Hime with normalized PDF . . . 13
9 Cylindrical Representation of Outer Detector . . . 14
10 Simulated Muon Daily Flux . . . 15
11 Muon Path Lengths Through OD . . . 15
12 Muon Path Lengths Through OD with Cryostat Removed . . . 16

Contents

I Introduction **3**

1 Preface **3**

2 Backgrounds **3**
2.1 Cosmogenic Backgrounds . . . 3
2.2 nEXO's Outer Detector . . . 4

3 Muon Spectra and Propogation **5**
3.1 Atmospheric Muons . . . 5
3.2 Muons Underground . . . 6

4 Cherenkov Light and Detection **7**

II Simulations **7**

5 Simulation Setup **8**
5.1 Muon Representation . . . 8
5.1.1 Muon Beam Positions . . . 9
5.1.2 Zenith Angle Sampling . . . 10
5.1.3 Limits of the Sample . . . 11
5.2 Outer Detector Representation . . . 11

6 Simple Simulation Outputs **12**
6.1 Parametric Intersection Points . . . 12
6.2 Overall Flux . . . 13
6.3 Muon Path Lengths . . . 14
6.4 Getting Fancy: Adding Cover Gas and Outer Cryostat . . . 14

Appendix A Numbers to Know **17**

Appendix B Iteratively Determining Maximum Zenith **17**

Appendix C Example Implementation **18**

Part I
Introduction

1 Preface

This work arose from an effort by nEXO's outer detector collaboration to deploy a GPU ray-tracing software to inform the geometric arrangement of the outer detector photomultiplier tubes (PMTs). The software, called *Chroma*, was written by SNO collaborators and has been largely used by other collaborations with experiments based at SNOLAB. Chroma takes as input detector geometry in the form of stl files and optical properties. Then, users must provide photon data for propagation. While Chroma, implemented in pyCuda, propagates photons at incredible speeds compared to previously used simulation tools, other physics processes must be dealt with externally.

The simulation of cosmogenic muons for nEXO was therefore necessary so that the resultant Cherenkov photons could be passed along to Chroma where they would subsequently be propagated. These through-going muons, having very high energies, were effectively treated as ray-like particles themselves. As the primary goal of the Chroma simulations was to judiciously position the photo-detectors, physics processes— as in the decay of muons or their spallation on nuclei— could safely be neglected as these would have a minimal effect on the produced Cherenkov light— the majority of which comes from the through-going muons. Thus, a simple muon Monte Carlo simulation was written with the primary purpose of creating accurate photon data with the added benefit of characterizing the anticipated flux.

This work seeks to document this muon simulation process by providing some background about backgrounds, outlining the necessity, referencing the applied formulae, and finally providing some example code to serve as a basis for future work.

2 Backgrounds

nEXO has an unprecented sensitivity reach to the $0\nu\beta\beta$ half life which requires radiologically pure construction materials and a build site impermeable to most cosmic rays. To meet and affirm these stringent requirements, nEXO collaborators deploy radiological assays to evaluate and select materials for purity. They then conservatively simulate the background impact due to the residual activity to yield an upper bound corresponding to the *background budget* [1]. The dominant backgrounds to nEXO are those arising from radioisotopes within detector materials including ^{238}U, ^{232}Th, ^{40}K and ^{60}Co. Moreover, ^{222}Rn presents a background both in the liquid xenon and in the cryogenic system.

2.1 Cosmogenic Backgrounds

There are also exogenous backgrounds to nEXO including those arising from cosmic rays; the mitigation of which requires building nEXO deep underground. The planned site for nEXO is SNOLAB's cryopit roughly 2 km or 5.89 km.w.e [1] underground where the isotropic muon flux is diminished by a factor of 2×10^8 [2]. However, while detector materials are at the surface (namely during manufacturing and testing phases), they undergo cosmogenic activation; thus a cool-down time underground is necessary before assembly. Without a great reduction in cosmic rays, nEXO's sensitivity would be unattainable. Even still, the residual muon flux contributes to the overall background by sending fast neutrons into the TPC or xenon filtration systems. Underground, gammas from local ^{238}U and ^{232}Th decays can give rise to background signals but mostly via the xenon filtration infrastructure external to the TPC [1].

$$^{136}\mathrm{Xe} + n \rightarrow ^{137}\mathrm{Xe} \tag{1}$$

$$^{137}\mathrm{Xe} \rightarrow ^{137}\mathrm{Cs} + \mathrm{e}^- + \bar{\nu}_e \tag{2}$$

[1] Kilometers of water equivalent— a unit of attenuation.

Free neutrons entering any one of nEXO's volumes containing liquid xenon can be captured by the liquid xenon producing ^{137}Xe which undergoes $\beta-$ decay with a half life of 3.82 minutes and a Q value spectrum extending into that of the known $2\nu\beta\beta$ [1]. Moreover, with sufficienct energy, these neutrons can even disintegrate nuclei sending other neutrons in their stead. Fast neutrons underground are primarily induced by muons. After passing through SNOLAB's overburden, muons may interact with local material to produce fast neutrons in the following ways [3]:

- Muon-induced nuclear disintegration
- Muon elastic scattering
- Photo-nuclear interactions
- A secondary process due to any of the above

2.2 nEXO's Outer Detector

nEXO is planned to be constructed with a water-Cherenkov outer detector (OD hereafter) surrounding the cryostat and internals. Taking the form of a large cylinder concentric with the TPC, it is to be instrumented with 127 PMTs at the time of writing. Its purpose is twofold. First, it shall passively shield the TPC from incident neutrons and gammas which are attenuated by the water. Second, it shall actively detect the Cherenkov light from through-going muons such that any affiliated signal is omitted in the final analysis—provided it meets the trigger conditions.

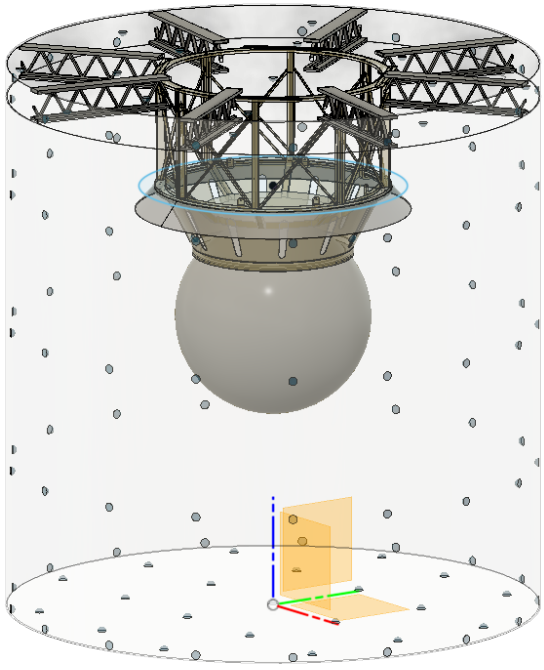

Figure 1: Fusion360$^{\text{TM}}$ Rendering of nEXO's Outer Detector

The OD will be filled with ultra pure water. At the time of writing, its radius is to be 617 cm and its height 1280 cm. Its PMTs will be inherited from the Daya Bay Reactor neutrino experiment; they are

8-inch diameter Hamamatsu^{TM} PMTs model R-5912. While there is still deliberation about the preferred construction materials, the internal surface of the OD is to be highly reflective to increase the likelihood of Cherenkov photons striking PMTs. There is also to be a layer of cover gas above the water kept at a positive pressure to ensure minimal contamination from foreign particulate.

3 Muon Spectra and Propogation

3.1 Atmospheric Muons

Cosmic ray muons are secondary particles in the cosmic ray ancestry- they arise from the decays of unstable primary cosmic rays, namely pions and kaons. At sea level, muons constitute the majority of charged cosmic rays with a flux of about 1 $cm^{-2}min^{-1}$ through the horizontal [4]. If you could *see* the muons, they would altogether look something like rain with each muon droplet travelling at relativistic speeds.

The flux of muons is not isotropic as muons with larger zenith angles are attenuated by more atmosphere. This introduces a selection mechanism relating the zenith distribution to that of the muon energy— muons traversing longer paths must have more energy in order to reach the point of measurement. The thickness of the atmosphere through which the muons must traverse is roughly related to the zenith angle, θ, by $1/\cos(\theta)$. See figure 2 for the measured energy spectra of muons at sea level. Notice how the shift in zenith angle moves the distribution to higher energies. Similar phenomena are observed underground.

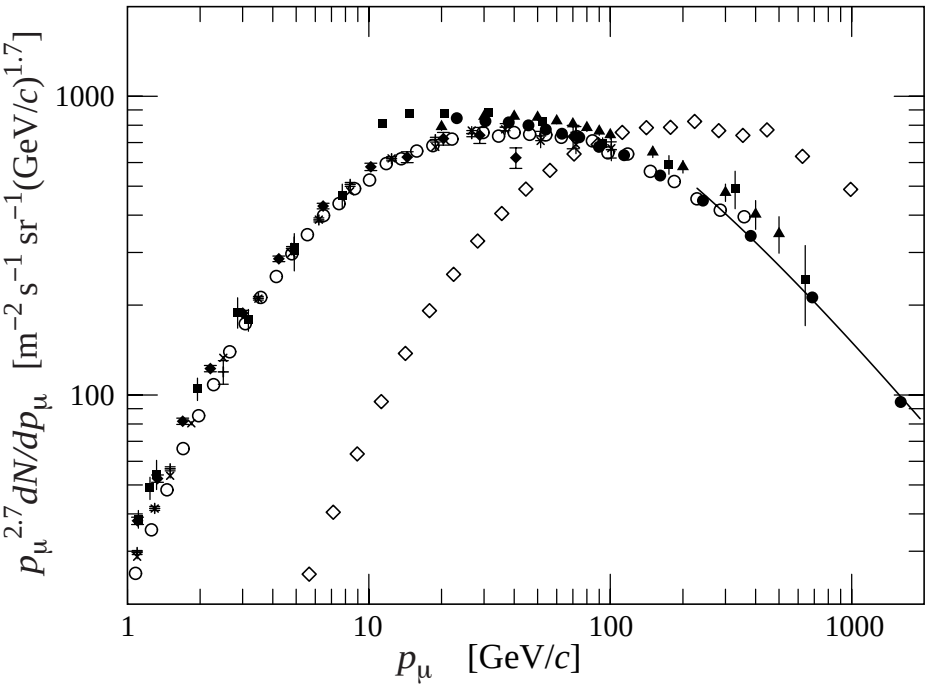

Figure 2: Atmospheric Muon Spectra; $\theta = 0°$ for ○, ▲, ■, ▼, ×, +. AND $\theta = 75°$ for ◇ [5]. The solid line is equation 3

Starting from the muon production spectra from atmospheric pions and kaons, Gaisser derived a double-differential relationship (with respect to energy and solid angle) for atmospheric muons based on both zenith angle and energy. Within the square brackets of equation 3, both the pion and kaon contributions are respectively represented. The relation is shown as the solid line in figure 2 [5] [6].

$$\frac{dN}{dE_\mu d\Omega} \simeq \frac{0.14 E_\mu^{-2.7}}{\text{cm}^2 \text{ s sr GeV}} \left[\frac{1}{1 + \frac{1.1 E_\mu \cos\theta}{115 \text{ GeV}}} + \frac{0.054}{1 + \frac{1.1 E_\mu \cos\theta}{850 \text{ GeV}}} \right] \tag{3}$$

3.2 Muons Underground

Of all the cosmic ray particles, only muons and neutrinos penetrate the Earth to considerable depths as they are not subject to strong interactions [5]. While neutrinos interact minimally with matter, the muons are attenuated by the Earth in a few processes. They suffer energy loss via ionization, electron-positron pair production, bremsstrahlung, and nuclear interactions [4]. For a more detailed overview of the radiative energy-loss processes of muons, the reader is referred to [7]. The attenuation of muons through matter can be given by the following relation:

$$-\frac{dE}{dx} = a(E) + b(E)E \tag{4}$$

where $a(E)$ describes the energy loss due to ionization and $b(E)$ describes the other processes including bremsstrahlung and pair production. For high energy muons, ionization is effectively constant ($a(E) \rightarrow$ constant) and bremsstrahlung dominates the attenuation processes [4]. At SNOLAB, muons have energies of roughly several hundred GeV thus bremsstrahlung dominates.

In addition, muons with larger zenith angles must travel through more of the overburden (rock probably) and thus, the zenith angle distribution narrows. Mei and Hime provide both depth and zenith angle intensity relations for laboratories of significant depth underground [8]. Mei and Hime's depth-intensity relation is given by equation 5 and shown in figure 3. The free parameters are given in appendix A. Notice the exponential decrease in muon intensity as a function of the depth- this makes SNOLAB an attractive site for high-sensitivity experiments like nEXO.

$$I(h) = I_1 e^{-h_0/\lambda_1} + I_2 e^{-h_0/\lambda_2} \tag{5}$$

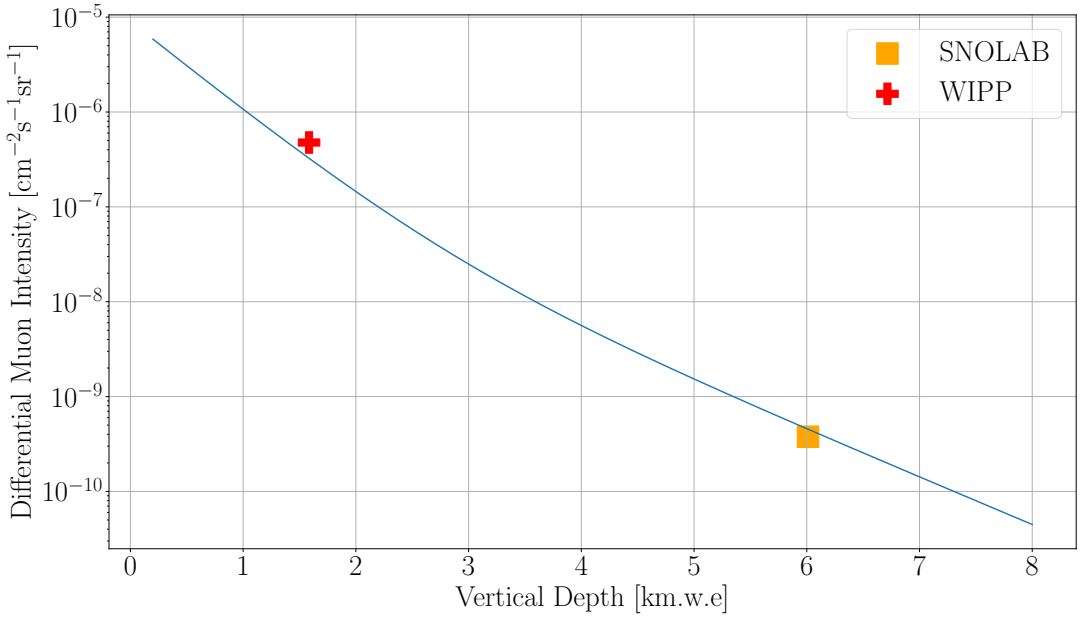

Figure 3: Mei & Hime's muon depth-intensity relation; Markers for WIPP and SNOLAB are shown. [8].

The energy of a muon is relevant as it is directly related to the amount of Cherenkov light produced as it passes through a water filled detector. However, this calculation requires a bit more thought as the muons have an energy distribution at the surface of the Earth, and then are attenuated according to their path lengths through the overburden. We would not expect *one* energy for any one zenith angle. Additionally, there is a threshold surface energy below which one would not expect muons to reach the detector. This is approximately 3 TeV for SNOLAB. The average energy of muons at SNOLAB is approximately 350 GeV. For simulations, the Gaisser approximation for high energies has often been used which relates a muon energy spectrum to an incident zenith angle [9]:

$$\frac{dN}{dE_0} \approx 0.14 E_0^{-2.7} [cm^{-2} s^{-1} sr^{-1} GeV^{-1}] \left(\frac{1}{1 + \frac{1.1 E_0 \cos\theta}{115 GeV}} + \frac{0.054}{1 + \frac{1.1 E_0 \cos\theta}{850 GeV}} \right) \tag{6}$$

The condition for the above distribution is that $E_\mu > (100 \text{ GeV} \,/\, \cos\theta)$. When sampling from a PDF for the muon energy, at SNOLAB, the minimum zenith angle will of course be 0, and the largest reasonable angle for muon flux is around 1 radian. Beyond this angle are fewer than 1% of muons (see appendix B).

4 Cherenkov Light and Detection

Cherenkov light is emitted whenever the velocity of a charged particle exceeds that of light in the medium through which it is passing [10]. If n is the index of refraction of the medium, β is the relativistic ratio, the speed criterion for the emition of Cherenkov light is:

$$\beta n > 1 \tag{7}$$

A Cherenkov detector, like nEXO's OD, works by detecting the emitted light with photomultiplier tubes (PMTs) optically coupled to the Cherenkov medium— water in our case. A Cherenkov photon liberates an electron on the PMT's photocathode and, using high magnitude electric fields, the PMT accelerates the initial photo-electron to create an *avalanche* of electrons which can be detected and translated into a digital signal.

Muons at SNOLAB have a mean energy measured at 363 GeV. Using the relativistic kinetic energy formula, we find $\beta_\mu \approx 1$. With the index of refraction of water being 1.33, our criterion is clearly met. Unlike isotropic scintillation light, Cherenkov light is emitted in the direction of the particle along the surface of a cone whose vertex angle is given by

$$\cos(\alpha) = \frac{1}{\beta n} \tag{8}$$

The Cherenkov light is not monochromatic, but rather follows a spectrum. This was first accurately described by Ilya Frank and Igor Tamm who won the 1958 Nobel Prize in Physics for the work (which was published in 1937) [11]. Their relation, quantifying Cherenkov light yield by wavelength and distance is [12]:

$$\frac{d^2N}{dx d\lambda} = \frac{2\pi\alpha z^2}{\lambda^2} \left(1 - \frac{1}{\beta^2 n^2(\lambda)} \right) \tag{9}$$

Where α is the fine structure constant, z the charge ratio of the particle to the elementary charge, β the relativistic speed ratio, and $n(\lambda)$ the wavelength-dependent index of refraction for the medium.

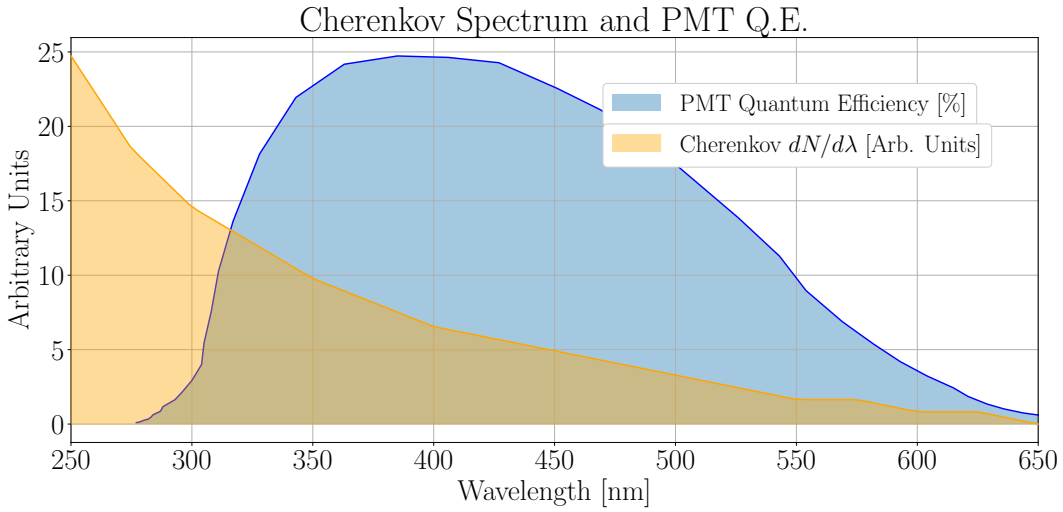

Figure 4: Cherenkov Spectrum for SNOLAB Muons with Hamamatsu R5912 Quantum Efficiency

Part II
Simulations

5 Simulation Setup

While muon spectra may be described by phenomenological distributions either at sea-level or underground, the stochastic nature of their interactions and the complexity of detector geometry make simulations the calculation tool to deploy. With random number generators at our disposal, we can model beams of particles such that they are pseudo-random on the individual level but converge to our model of choice on the aggregate. How do we begin? Let us take up the case of simulating a beam of muons as if we are underground at SNOLAB focussed on nEXO's outer detector. We won't worry about the physics, but simply the transportation of the logical particles and their intersections with our virtual detector.

5.1 Muon Representation

There are several things that need to be logically represented when defining a beam of particles. For instance, the position, direction, and energy of the beam must be defined. Moreover, the coordinate systems of beam and detector must be clearly related. To that end, a basic muon requires at least six numbers to be accurately represented; three for momentum in each direction, and three to define some reference position, say, the starting point of the particle. For muons, the momentum must be treated relativistically and so it is more simple to maintain energy, direction, and starting position as the three parameters of the muon. Seven numbers in all:

$$\mu = \begin{bmatrix} E_\mu & \mu_x & \mu_y & \mu_z & x_0 & y_0 & z_0 \end{bmatrix} \tag{10}$$

However, for easier representation, we find it judicious to represent a muon using spherical coordinates to define the direction- cartesian direction vectors can be simply derived from these. Further, these angles are more simply generated in the simulation as we'll see. A muon becomes:

$$\mu = \begin{bmatrix} E_\mu & \theta & \phi & x_0 & y_0 & z_0 \end{bmatrix} \tag{11}$$

5.1.1 Muon Beam Positions

First, one must define where exactly the particles are coming from. This isn't as trivial as it sounds, as the muons should all be coming from different directions and the coordinate frame of the detector must be related to that of the muons. It's judicious to lay the spatial ground rules from the get-go. Already, one requires 3 numbers to express the beam "starting position". For the sake of the muon simulations, we exploit the azimuthal symmetry of nEXO's outer detector and instantiate the muons on a disk somewhere above it. We can simply set all starting positions to have the same z coordinate and determine x and y randomly. The choice of z will be clarified in a later section.

One can sample points uniformly on a disk using polar coordinates. Only two numbers must be randomly generated, the radius and the polar angle. We know that

$$R^2 = x^2 + y^2 \tag{12}$$

$$x = R\cos\theta \quad \text{and} \quad y = R\sin\theta \tag{13}$$

So one might think to generate a random number from 0 to R for the radius and one from 0 to 2π for the polar angle. This is semi-correct. Figure 5 shows two resultant distributions, one of which— the wrong one— results from this approach. The distribution is not uniform across the disk, whereas the right version has the uniformity we desire. To achieve this, we must generate a random number ρ from 0 to R^2, a random number θ from 0 to 2π, and determine x and y from

$$x = \sqrt{\rho}\cos\theta \quad \text{and} \quad y = \sqrt{\rho}\sin\theta \tag{14}$$

Paul J. Nahin discusses these methods in his book *Digital Dice* [13]. In essence, it can be described by the proportionality of a differential element of area to the radius; as R increases, so does the area element $Rd\theta dR$. Thus, one must maintain a uniform distribution in R^2 which is skewed towards greater R.

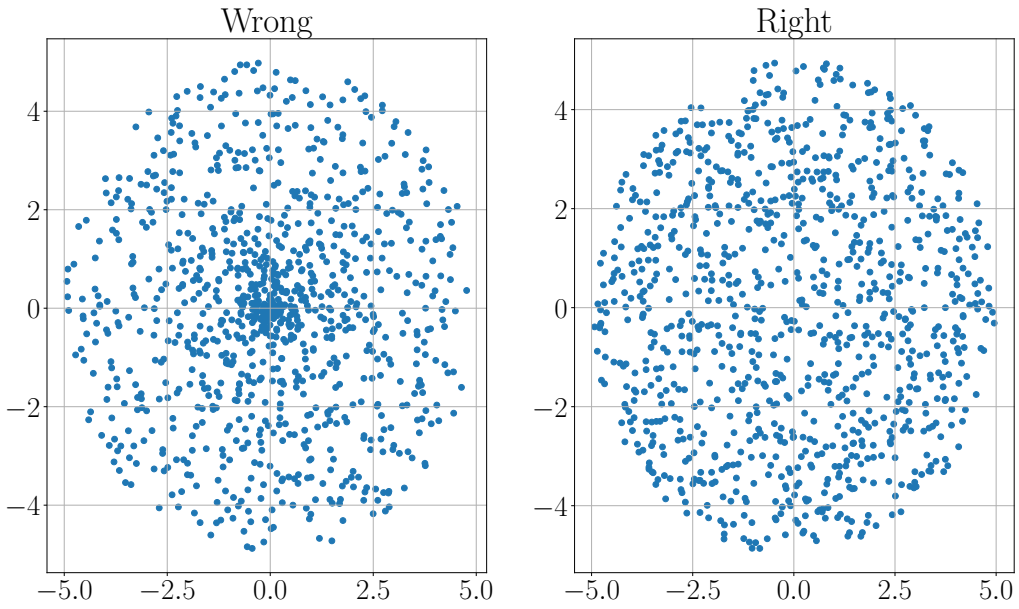

Figure 5: Non-uniform and uniform spatial distributions with random polar numbers.

ρ is the radius of the virtual disk on which we generate the muons. So what should ρ be? As we'll see, we choose to represent the OD as a cylinder centered at the origin (this reference is arbitrary) and our criterion depends on how much of the muon zenith spectrum we wish to simulate. Figure 6 shows a diagram of the virtual OD and generating disk whose parameters will be judiciously chosen in the next section.

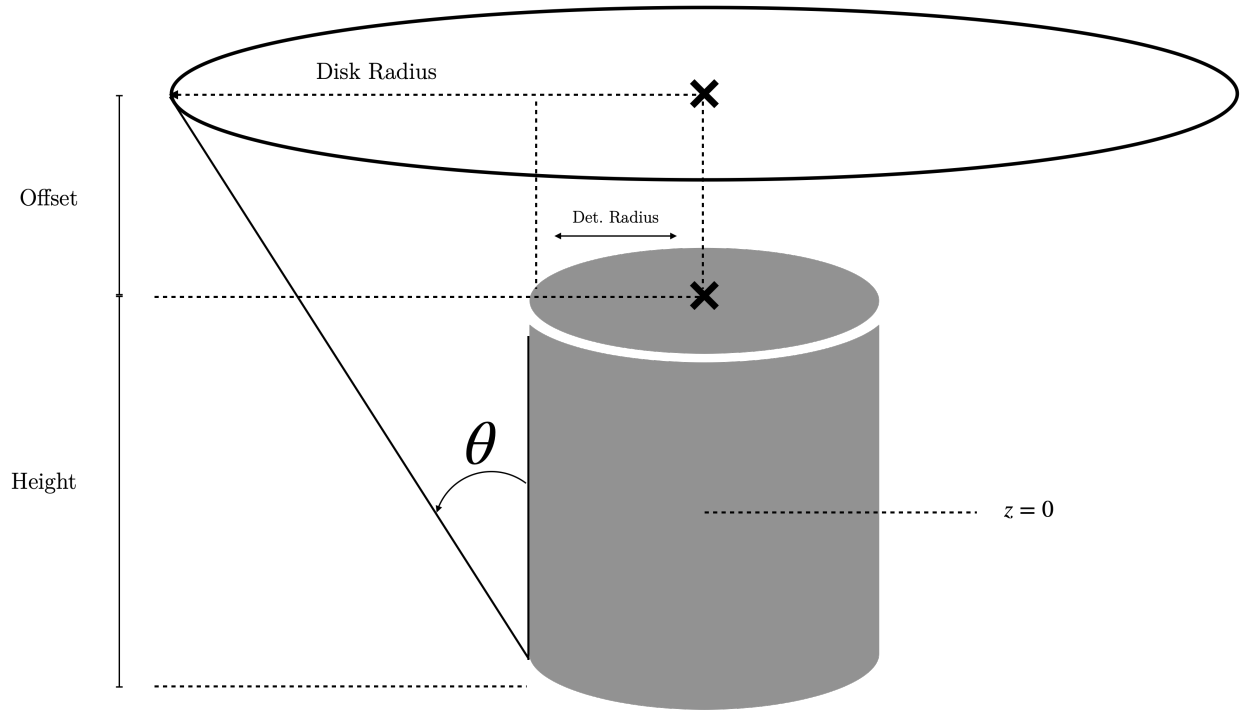

Figure 6: Criterion angle θ to determine disk radius.

In summary, there are three critical things to consider when defining the instantiation positions for this specific beam. The first is to confirm the uniformity of the distribution about the disk, the second is to ensure the disk size makes sense, and finally, that the coordinates of the instantiation points are related to the detector in the expected way.

5.1.2 Zenith Angle Sampling

As mentioned, the flux of muons and their energies are directly related to the zenith angle from which they are measured. This is true at sea-level where muons are attenuated by the atmosphere as it is true underground where muons are attenuated by the overburden of rock. Mei and Hime quantify the zenith angle relations for a given angle at a given depth by changing the vertical depth h_0 of equation 5 for the **slant-depth**, $h = h_0 \sec\theta$ and by multiplying by $\sec\theta$. The result converts equation 5 to one providing the through-going muon intensity at a given zenith angle and depth:

$$I_{\text{th}}(h_0, \theta) = (I_1 e^{-h_0/\lambda_1 \cos(\theta)} + I_2 e^{-h_0/\lambda_2 \cos(\theta)})/\cos(\theta) \qquad [\text{cm}^{-2}\text{sr}^{-1}\text{s}^{-1}] \tag{15}$$

We must note that the above equation (15) is an isotropic distribution. If one wishes to determine the flux through a horizontal plane, the equation must be projected onto the horizontal. Noting the units, we must multiply by the differential solid angle $d\Omega = \sin(\theta) d\theta d\phi$ and by $\cos(\theta)$. Figure 8 shows both the normalized equation 15, and its projection onto the horizontal. It becomes:

$$\frac{dI_{\text{th}}(h_0, \theta)}{d\theta} = 2\pi(I_1 e^{-h_0/\lambda_1 \cos(\theta)} + I_2 e^{-h_0/\lambda_2 \cos(\theta)}) \sin(\theta) \qquad [\text{cm}^{-2}\text{s}^{-1}] \tag{16}$$

The above differential intensity function can be normalized and used as a PDF from which zenith angles may be sampled for the generated muons.

5.1.3 Limits of the Sample

At this point, we refer to figure 6 in defining the generation parameters. How big must the radius be? How should one determine the offset of the generation disk? Of course, these parameters are related and depend principally on the chosen largest zenith angle, θ_m, which we are free to choose. While one could sample all the way to $\pi/2$, realistically, the relative likelihood of this angle is nill, and to even witness a muon with that angle pass through the OD, a generation disk must extend radially to infinity. So, the distribution must be bound. Say, for instance, we decide we can safely neglect 1% of muons, then we must determine which angle, as the upper limit of integration, encompasses 99% of equation 16. With A being a normalization constant, we have:

$$A\int_0^{\theta_m}(I_1e^{-h_0/\lambda_1\cos(\theta)}+I_2e^{-h_0/\lambda_2\cos(\theta)})\sin(\theta)d\theta=0.99 \tag{17}$$

This integral is non-trivial to say the least. To determine θ_m, we can deploy the Newton-Raphson method as seen in appendix B. Finding a solution of 1.047 radians for 95% zenith angle coverage, we can use this criterion angle, and the geometry of the configuration in figure 6 to define the minimum disk radius with the following equation:

$$R_{\text{min}}\geq R_{\text{OD}}+(h_{\text{OD}}+\text{offset})\tan\theta \tag{18}$$

The next query has to do with the choice of disk offset. This choice requires careful consideration; if the muons are to be attenuated, or spallation processes are to be simulated, how much of an overburden is necessary for the accurate characterization of these phenomena? These questions are beyond the scope of this work.

However, if we generate muons at a constant areal rate on the disk (say 1 per cm^2), we expect to witness a linear decrease with the offset if we leave the disk radius constant. If instead we vary R_{disk} with the offset according to equation 18, we should expect only statistical fluctuations. Indeed, we witness just this phenomenon in figure 7 where for one series, the radius was fixed, and for the other, it was varied proportionally to the offset according to equation 18. For the figure, the muons were generated at a rate of 100 per square meter on the disks.

5.2 Outer Detector Representation

The outer detector is a cylinder underneath a flat overburden. We are free to exploit the azimuthal symmetry of the problem. In order to define a cylinder with parametric equations, two (or three) sets of equations are necessary. The first, equation 19, defines the cylinder column; the second, equation 20, defines circles which form the top or bottom of the cylinder centred at the origin. See figure 5.2 for a representation of this cylinder in 3-space. The choice of origin is arbitrary, but must be consistently referenced throughout.

$$\begin{pmatrix}x\\y\\z\end{pmatrix}=\begin{pmatrix}R\cos u\\R\sin u\\v\end{pmatrix}\ \text{with } v\in[-\frac{h}{2},\frac{h}{2}]\text{ and } u\in[0,2\pi] \tag{19}$$

$$\begin{pmatrix}x\\y\\z\end{pmatrix}=\begin{pmatrix}t\cos u\\t\sin u\\\pm h/2\end{pmatrix}\ \text{with } t\in[0,R]\text{ and } u\in[0,2\pi] \tag{20}$$

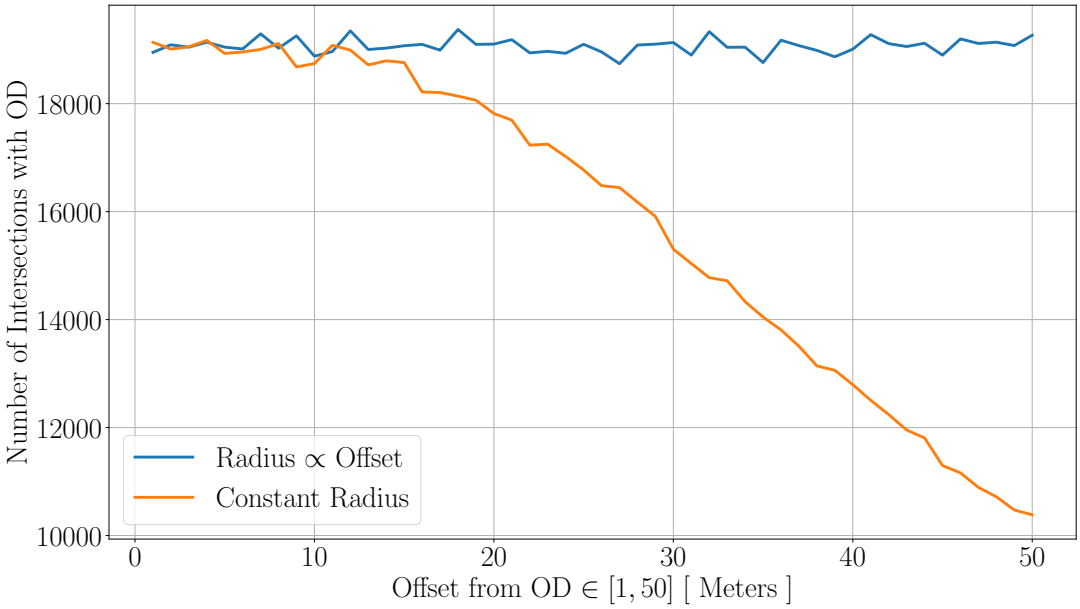

Figure 7: Number of muon intersections vs. generation disk offset

6 Simple Simulation Outputs

6.1 Parametric Intersection Points

The outer detector may be represented with parametric equations, and so too may the muon track. The parametric muon track takes the following form:

$$\begin{pmatrix} x \\ y \\ z \end{pmatrix} = \begin{pmatrix} m_x q + x_0 \\ m_y q + y_0 \\ m_z q + z_0 \end{pmatrix} \quad \forall \ q \tag{21}$$

We take the slope values of the parametric line to be the values of a unit vector of the muon path, and the zero values to be the muon starting point:

$$\vec{\mu} = \begin{pmatrix} m_x \\ m_y \\ m_z \end{pmatrix} = \begin{pmatrix} \sin\theta\cos\phi \\ \sin\theta\sin\phi \\ -\cos\theta \end{pmatrix} \quad \text{and} \quad \mu_0 = \begin{pmatrix} x_0 \\ y_0 \\ z_0 \end{pmatrix} \tag{22}$$

Finally, the muon track in parametric form is given by:

$$\vec{\mu} q + \mu_0 = \begin{pmatrix} m_x q + x_0 \\ m_y q + y_0 \\ m_z q + z_0 \end{pmatrix} \quad \forall \ q \tag{23}$$

The OD and muon track parametric equations can be used to determine a muon's intersection points with the outer detector. We can first check for intersection with the top and bottom by solving the linear equations for where $z = \pm h/2$ (based on the OD centred at the origin). Solving for q, we can confirm whether or not x and y are within the circle of the cylinder:

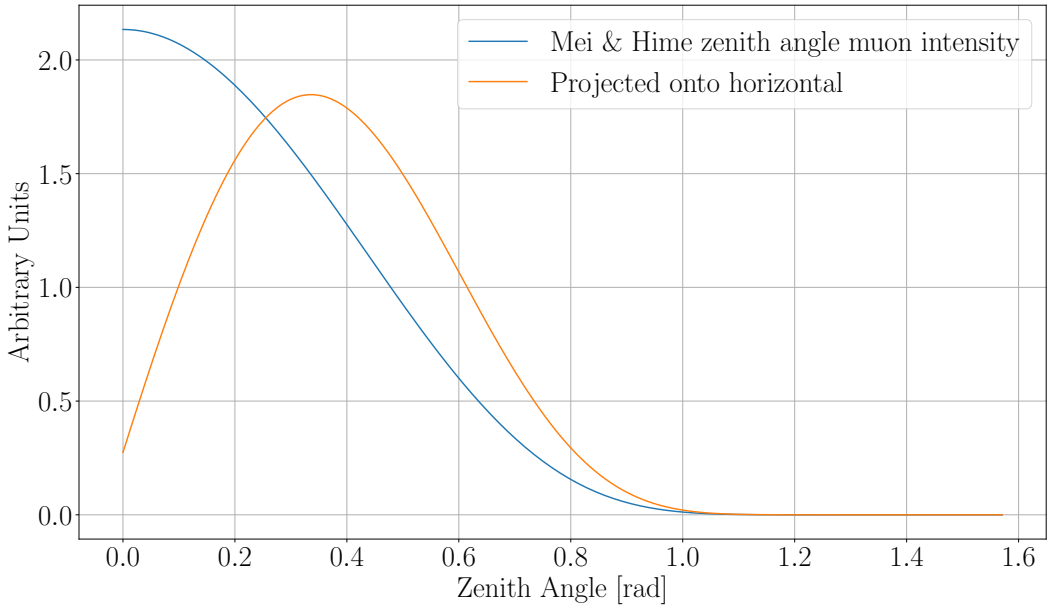

Figure 8: Equation 15 as is, and projected onto the horizontal. Both are normalized.

$$q = \frac{\pm h/2 - z_0}{m_z} = \frac{\pm h/2 - z_0}{(-\cos\theta)} \tag{24}$$

Next, we can check if the muon intersects the side of the detector (and where) by solving the equation:

$$x^2 + y^2 = R^2 \tag{25}$$

which becomes the quadratic equation:

$$(m_x^2 + m_y^2) \cdot q^2 + 2(x_0 m_x + y_0 m_y) \cdot q + (x_0^2 + y_0^2 - R^2) = 0 \tag{26}$$

If implemented in this way, the determinant can be used to determine whether or not the muon track hits the side of the OD, and if it does, there may be two solutions. The smaller q value corresponds to the point at higher z.

6.2 Overall Flux

The previous section lays the groundwork for the simulation outputs that lie ahead. Once we can efficiently determine the intersection points of muon tracks with the OD, we can deploy the program for determining the overall muon flux through the OD as a function of time. This is fairly simple to do, we simply instantiate a large number of muons on a disk and then scale the estimated flux by the ratio of our generation rate on the disk to a measured value for horizontal flux. We obviously need to know the area of the disk. In our case, we use SNOLAB's measured number of 3.31×10^{-10} $\mu\ cm^{-2}\ s^{-1}$.

A different approach would be to determine the daily flux by the previous method for a large number of days. The result is a normal distribution. In our case, the distribution is shown in figure 10 and fitted with a Gaussian for which the mean is 54.27 muons per day. This distribution comprises 30 years of simulated days of through-going muons.

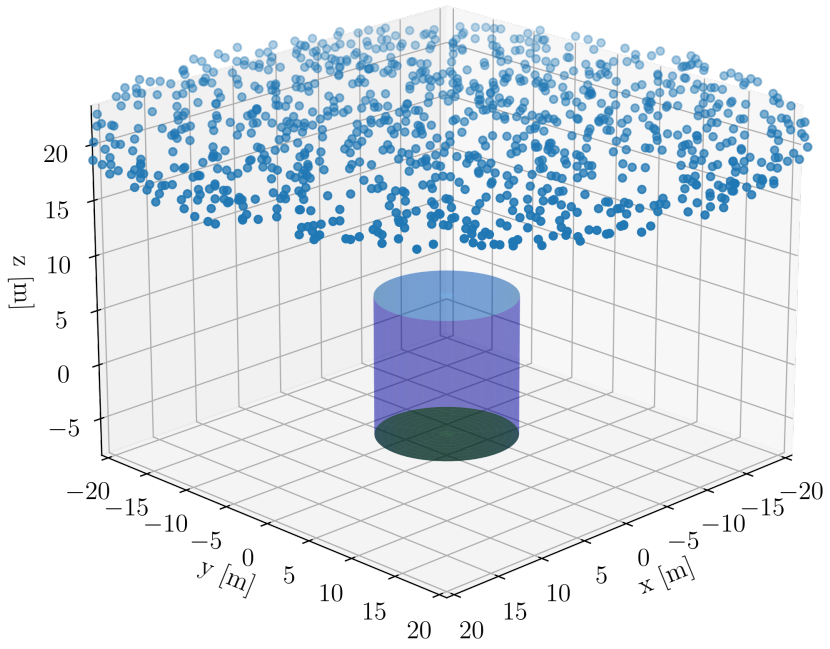

Figure 9: Outer detector cylinder centered at origin with muon instantiation points above it on a disk.

6.3 Muon Path Lengths

Not only can we deduce the muon flux rate, we can also determine the path lengths of the muons through the outer detector. Our parametric equations from earlier give us exact entry and exit positions. These path lengths can allow us to determine the expected number of Cherenkov photons and potentially how they would be dispersed. The path length distribution for 5×10^4 muons is shown in figure 11. The figure also discriminates between the characteristic entry and exit points of the muons. For instance, those muons having paths through the top and bottom of the OD have a histogram in blue. We see the lowest value for this pathlength is the height of the OD.

6.4 Getting Fancy: Adding Cover Gas and Outer Cryostat

A few other details which would be judicious to add for path length concerns are the outer cryostat (OC) and the cover gas. The OC can be approximated as a sphere within the OD. Muons tracks would not send Cherenkov light from within the OC, and therefore to properly account for this unseen light, it's instrumental that the OC be added in the configuration. Fortunately for the OC, this requires only solving another small set of equations. Additionally, the cover gas layer is also simple to account for, as it just shortens the water column within the OD. The surface of the OC is given by:

$$x^2 + y^2 + z^2 = R_{\text{cryo}}^2 \tag{27}$$

From which we can deduce the muon intersection points (if any) if we know the outer cryostat position: $P_{\text{cryo}} = \begin{pmatrix} x_{\text{cryo}} & y_{\text{cryo}} & z_{\text{cryo}} \end{pmatrix}$. With the muon parametrized as in equation 23, we are left to solve a quadratic equation for the muon parameter q :

$$q = \frac{-B \pm \sqrt{B^2 - 4AC}}{2A} \tag{28}$$

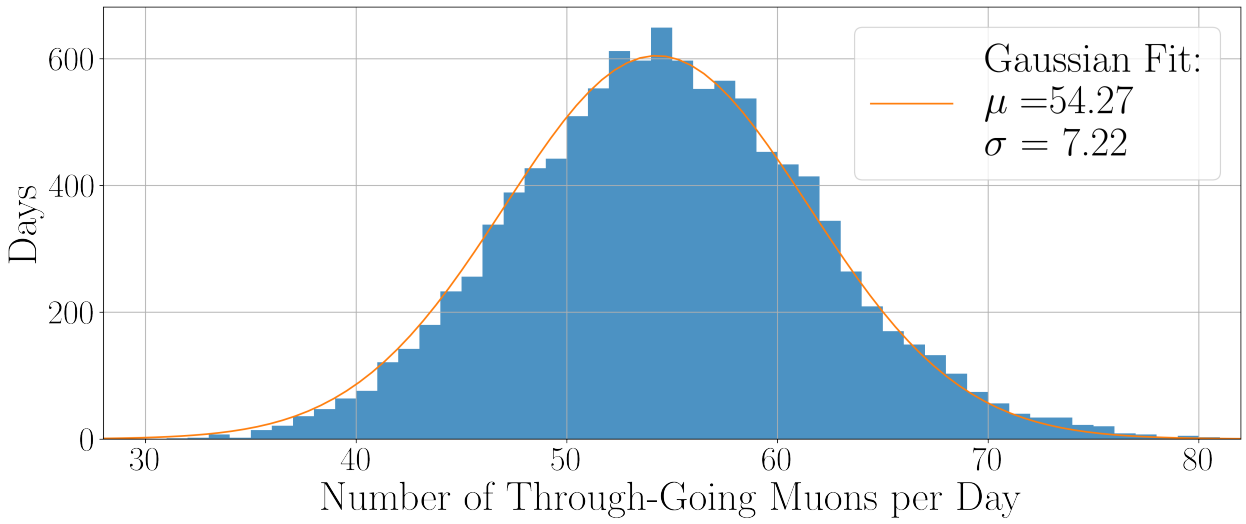

Figure 10: 30 years of daily counts of through going muons in the OD.

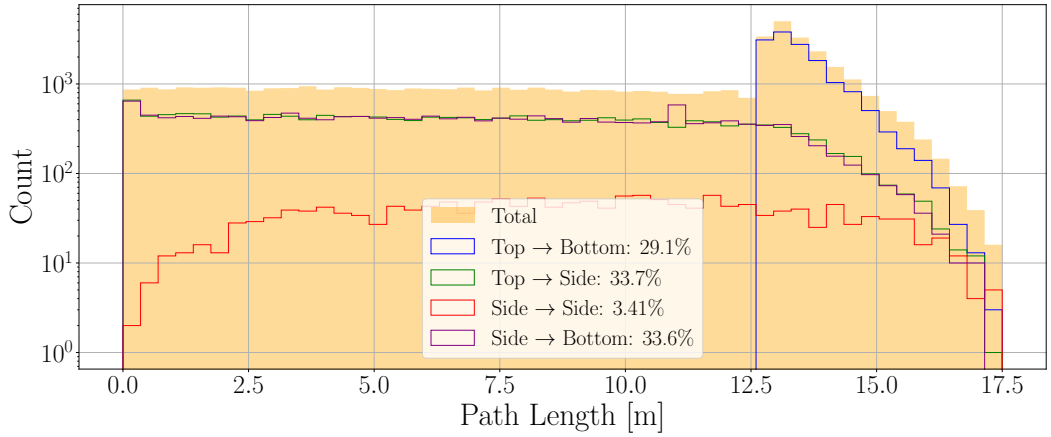

Figure 11: 50000 through-going muon paths in the OD characterized by their entry and exit points

where

$$A = \sum m_i^2 \qquad i \in [x, y, z]$$
$$B = 2\sum (m_i i_0 - m_i i_{\text{cryo}}) \qquad i \in [x, y, z]$$
$$C = \sum (i_0^2 + i_{\text{cryo}}^2 - i_0 i_{\text{cryo}}) \qquad i \in [x, y, z]$$

Such that the muon's intersection points with the OC are given by

$$P_{(\mu-\text{cryo})} = \begin{pmatrix} qm_x + x_0 & qm_y + y_0 & qm_z + z_0 \end{pmatrix} \tag{29}$$

Adding a spherical OC to the configuration alters the path length output. Particularly we notice a more rounded histogram for the top-bottom type entry and exit points with the minmum now extending to the difference between the detector height and the OC diameter.

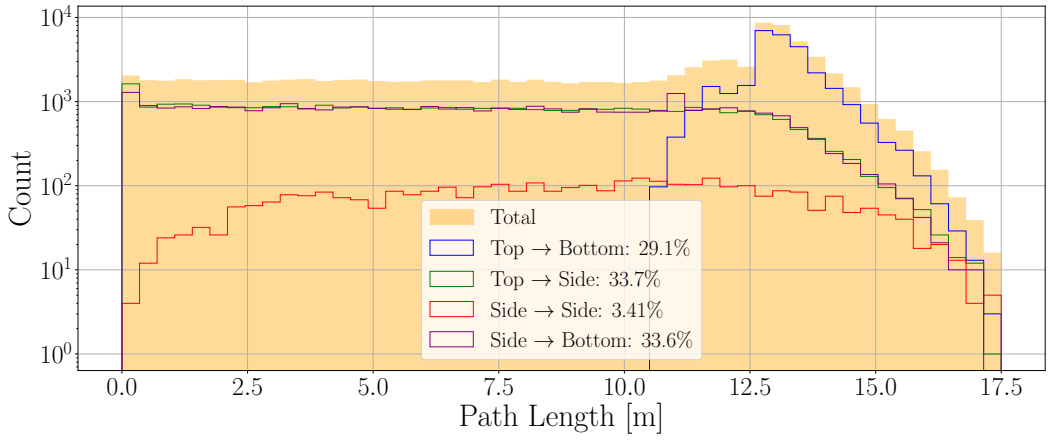

Figure 12: 50000 through-going muon paths in the OD characterized by their entry and exit points- cryostat removed

Appendices

Appendix A Numbers to Know

Mei & Hime's Depth Intensity Relation [8]		
Parameter	Value	Units
I_1	$(8.60 \pm 0.53) \times 10^{-6}$	$s^{-1}cm^{-2}sr^{-1}$
λ_1	(0.45 ± 0.01)	km.w.e
I_2	$(0.44 \pm 0.06) \times 10^{-6}$	$s^{-1}cm^{-2}sr^{-1}$
λ_2	(0.87 ± 0.02)	km.w.e
h_0	Vertical Lab Depth	km.w.e

SNOLAB Specific Numbers			
Parameter	Value	Units	Source
h_0	5.89 ± 94	km.w.e	[14]
Φ_μ	$(3.31 \pm 0.01(\text{stat}) \pm 0.09(\text{sys})) \times 10^{-10}$	μ cm^{-2} s^{-1}	[2]
E_μ	363.0 ± 1.2	GeV	[2]

Appendix B Iteratively Determining Maximum Zenith

We would like to find the maximum zenith angle, θ_m, to determine the breadth of angles to sample from in equation 16. We have an integral with a complicated integrand and must determine the upper bound that yields our chosen constant— the fraction of angles we wish to see represented in the simple Monte Carlo.

$$A \int_0^{\theta_m} (I_1 e^{-h_0/\lambda_1 \cos(\theta)} + I_2 e^{-h_0/\lambda_2 \cos(\theta)}) \sin(\theta) d\theta = L \tag{30}$$

Our problem is easily tackled with Newton's method [15], but we must rephrase it. It becomes a root finding exercise.

$$x_{n+1} = x_n - \frac{F(x_n)}{F'(x_n)} = x_n - \frac{1}{f(x_n)} \left(\int_0^{x_n} f(\theta)\, d\theta - L \right) . \tag{31}$$

And in our case:

$$f(x) = A(I_1 e^{-h_0/\lambda_1 \cos(\theta)} + I_2 e^{-h_0/\lambda_2 \cos(\theta)}) \sin(\theta) d\theta - L \tag{32}$$

Now we need only iterate through until the desired tolerance is reached. A judicious first guess would be $x_0 \in [0, \pi/2)$. In Python, we can find the solution using Scipy's "newton" function. The following code finds an angle of 1.047 radians for 95% angle coverage:

```
def find_max_angle(level = 0.95, tolerance = 0.001):
    from scipy.optimize import newton
    from scipy.integrate import quad
    from numpy import exp, sin, cos, pi

    # Define constants used through functions
    I1 = 8.60e-6
    lam1 = 0.45
    I2 = 0.44e-6
    lam2 = 0.87
    vdepth = 5.89

```

```
    # Define our function as a callable lambda function object
    func = lambda x : (I1*exp(-vdepth/(lam1*cos(x))) \
        + I2*exp(-vdepth/(lam2*cos(x))))*sin(x)

    # Define normalization constant
    A = 1/quad(func, 0, pi/2)[0]

    # Define normalized function
    func_normd = lambda x : A*(I1*exp(-vdepth/(lam1*cos(x))) \
        + I2*exp(-vdepth/(lam2*cos(x))))*sin(x) - level

    # Determine the max angle
    max_angle = newton(func_normd, pi/3, tol= tolerance)  # Radians

    return max_angle
```

Appendix C Example Implementation

The following is an example of a muon class implemented in Python.

```
class Muon:
    '''
    A class for muons parameterized by empirical functions.

        - zenith                [rad]
        - azimuth               [rad]
        - energy                [GeV]
        - initial_position      [meters, meters, meters]
        - rest_mass_kg          [kg]
        - rest_mass_MeV         [MeV/c^2]
    '''

    # Attribute of the class:
    rest_mass_kg = 1.8835e-28   # [kg]
    rest_mass_MeV = 105.66      # [MeV]
    charge = 1.60218e-19        # [C]

    def __init__(self, zenith=0, azimuth=0, energy=SNOLAB_MU_E_AVG, initial=(0,0,0)) -> '
        Muon':
        ''' A constructor for the muon. Defaults to vertical muon at average SNOLAB energy
            '''

        self.zenith = zenith
        self.azimuth = azimuth
        self.energy = energy
        self.initial = initial


    ### Instance Functions

    def get_unit_vec(self) -> tuple:
        ''' Returns a unit vector for the muon direction (x,y,z)'''

        x = np.sin(self.zenith)*np.cos(self.azimuth)
        y = np.sin(self.zenith)*np.sin(self.azimuth)
        # Muons are going DOWN
        z = -np.cos(self.zenith)

        return (x,y,z)

    def get_cartesian_track(self) -> tuple:
        ''' Returns the muon track (x, y, z, x0, y0, z0)'''

        return self.get_unit_vec()+self.initial

    def closest_approach(self, point):
```

```
45          ''' Finds the muon's closest distance to the provided point in 3-space (cartesian
                coords)'''
46
47          unit_vector = self.get_unit_vec()
48
49          # Parameterize for simplicity
50
51          i, j, k = point[0], point[1], point[2]
52          mx, my, mz = unit_vector[0], unit_vector[1], unit_vector[2]
53          x0, y0, z0 = self.initial[0], self.initial[1], self.initial[2]
54
55          t = ((mx*i + my*j + mz*k) - (mx*x0 + my*y0 + mz*z0))/(mx**2 + my**2 + mz**2)
56
57          muon_point = (mx*t + x0, my*t + y0, mz*t + z0)
58
59          x_dist = muon_point[0] - i
60          y_dist = muon_point[1] - j
61          z_dist = muon_point[2] - k
62
63          distance = np.sqrt(x_dist**2 + y_dist**2 + z_dist**2)
64
65          return distance
```

References

[1] G. Adhikari et al., Journal of Physics G: Nuclear and Particle Physics **49** (2021).

[2] B. Aharmim et al., Phys. Rev. D **100** (2019).

[3] Y.-F. Wang et al., Phys. Rev. D **64**, 013012 (2001).

[4] C. Grupen, *Astroparticle Physics*, Undergraduate Texts in Physics, Springer, 2020.

[5] P. Zyla et al., PTEP **2020**, 083C01 (2020), and 2021 update.

[6] T. K. Gaisser, *Cosmic rays and particle physics*, Cambridge University Press, Cambridge, United Kingdom, second edition. edition, 2016.

[7] D. E. GROOM, N. V. MOKHOV, and S. I. STRIGANOV, Atomic Data and Nuclear Data Tables **78**, 183 (2001).

[8] D.-M. Mei and A. Hime, Phys. Rev. D **73**, 053004 (2006).

[9] J. Albert et al., Journal of Cosmology and Astroparticle Physics **2016**, 029 (2016).

[10] G. F. Knoll, *Radiation detection and measurement / Glenn F. Knoll.*, J. Wiley, New York, 4th ed. edition, 2010.

[11] I. Frank and I. Tamm, Coherent visible radiation of fast electrons passing through matter, in *Selected Papers*, pages 29–35, Springer Berlin Heidelberg, 1991.

[12] P. Zyla et al., PTEP **2020**, 083C01 (2020), in section *Passage of particles through matter*.

[13] P. J. Nahin, *Digital dice : computational solutions to practical probability problems*, Princeton University Press, Princeton, 2008.

[14] B. Aharmim et al., Physical Review D **80** (2009).

[15] M. J. Maron, *Numerical analysis : a practical approach*, Wadsworth Pub. Co., Belmont, Calif, 3rd ed. edition, 1991.